Structure of xylose reductase bound to NAD$^+$ and the basis for single and dual co-substrate specificity in family 2 aldo-keto reductases

Kathryn L. KAVANAGH*, Mario KLIMACEK†, Bernd NIDETZKY† and David K. WILSON*[1]

*Section of Molecular and Cellular Biology, University of California, Davis, CA 95616, U.S.A., and †Institute of Biotechnology, Graz University of Technology, Petersgasse 12, A-8010 Graz, Austria

Xylose reductase (XR; AKR2B5) is an unusual member of aldo-keto reductase superfamily, because it is one of the few able to efficiently utilize both NADPH and NADH as co-substrates in converting xylose into xylitol. In order to better understand the basis for this dual specificity, we have determined the crystal structure of XR from the yeast *Candida tenuis* in complex with NAD$^+$ to 1.80 Å resolution (where 1 Å = 0.1 nm) with a crystallographic *R*-factor of 18.3 %. A comparison of the NAD$^+$- and the previously determined NADP$^+$-bound forms of XR reveals that XR has the ability to change the conformation of two loops. To accommodate both the presence and absence of the 2′-phosphate, the enzyme is able to adopt different conformations for several different side chains on these loops, including Asn^{276}, which makes alternative hydrogen-bonding interactions with the adenosine ribose. Also critical is the presence of Glu^{227} on a short rigid helix, which makes hydrogen bonds to both the 2′- and 3′-hydroxy groups of the adenosine ribose. In addition to changes in hydrogen-bonding of the adenosine, the ribose unmistakably adopts a 3′-*endo* conformation rather than the 2′-*endo* conformation seen in the NADP$^+$-bound form. These results underscore the importance of tight adenosine binding for efficient use of either NADH or NADPH as a co-substrate in aldo-keto reductases. The dual specificity found in XR is also an important consideration in designing a high-flux xylose metabolic pathway, which may be improved with an enzyme specific for NADH.

Key words: crystal structure, enzyme specificity, NADH, NADPH, xylose fermentation.

INTRODUCTION

Xylose reductase (XR) from *Candida tenuis* (AKR2B5) is a 322 amino acid 36 kDa protein that is capable of reducing the open-chain form of D-xylose to the corresponding polyol xylitol by utilizing either an NADPH or NADH co-substrate [1]. It belongs to family 2 of the aldo-keto reductase (AKR) superfamily which is made up of 14 different families and approx. 120 members [2]. Its homodimeric nature is unusual for AKRs, since the majority of these are functional as monomers. Also unusual is its ability to efficiently utilize either co-substrate [3]. Some of the AKRs such as XR have well-characterized functions, involving xenobiotic, steroid, sugar, polyketide and vitamin metabolism as well as detoxification of reactive aldehydes. The physiological purpose of many others remains unknown or speculative. Despite this, the development of inhibitors for AKRs, including human aldose reductase (AR; AKR1B1), has been a goal for many years [4].

The crystal structure of XR has been determined previously to 2.2 Å resolution (where 1 Å = 0.1 nm) in both apo- and NADP$^+$-bound forms [5]. As seen in the structures of other AKRs, the protein folds into a $(\beta/\alpha)_8$ barrel, the most common motif seen for enzymes [6]. The protein dimerizes using an unusual hydrophilic patch consisting of residues from loop 4, the loop connecting strand 4 with helix 4 as well as interactions from helices 5 and 6 and the C-terminal loop. These orient the active sites of the dimer in an approximately anti-parallel conformation. The co-substrate binds across the face of the barrel and helps to form the carbonyl-containing substrate-binding site. These structures explain the kinetically observed ordered mechanism where the co-substrate binds before the carbonyl-containing substrate and dissociates last [3].

As xylose is a sugar found in abundance in plant cell walls and biomass, an efficient method of converting this into ethanol would be an environmentally preferable method of disposal of many agricultural wastes [7]. XR catalyses the first step of a pathway that allows certain organisms to metabolize xylose. After the reduction of xylose to xylitol by XR in a manner which can utilize NADH ($K_m = 25.4$ μM; $k_{cat} = 18.1$ s^{-1}) or NADPH ($K_m = 4.8$ μM; $k_{cat} = 21.9$ s^{-1}), xylitol is re-oxidized to yield xylulose by xylitol dehydrogenase, which is often specific for NAD$^+$ [8]. Xylulose can then be phosphorylated and enter general metabolic pathways. An efficient, high-flux pathway should recycle the co-substrate such that there is no net conversion of NADPH into NADH resulting from xylose metabolism. Perturbations in this ratio have been linked to cellular stress and xylitol excretion [9]. An XR that is exclusively specific for NADH could alleviate this problem. It has been noted previously [9a] that the potential bottleneck in a high-flux pathway may be in the pentose phosphate pathway, transaldolase or transketolase reactions. Improvements in the XR k_{cat} values are unlikely to be useful at this point, but may become significant if these limitations are removed in the future [10]. The structure of XR was determined previously in apo form as well as complexed with the NADP$^+$ co-substrate [5]. To provide a basis for mutants that might exhibit enhanced NADH specificity, we have determined the structure of XR in a binary complex with the alternative co-substrate NAD$^+$. In order to understand the co-substrate

Abbreviations used: AKR, aldo-keto reductase; AR, human aldose reductase; r.m.s., root mean square; XR, xylose reductase.

[1] To whom correspondence should be addressed (e-mail dave@alanine.ucdavis.edu).

The co-ordinates reported have been submitted to the Protein Data Bank under accession number 1MI3.

specificity in XR and other members of the superfamily, we have compared this structure with the NADP$^+$-bound structure of other AKRs that are specific for NADPH.

Attempts to modify co-substrate specificity have improved the catalytic efficiency of *Corynebacterium* 2,5-diketo-D-gluconic acid reductase A, a member of the AKR family 5, approx. 7-fold for NADH [11]. The effects of mutations on residues making salt links with the 2′-phosphate have also been examined in AR [12] and human 3α-hydroxysteroid dehydrogenase [13,14]. Both of these experiments indicate that, although the specificity for the 2′-phosphate may be affected by these interactions, it is not solely governed by them. In almost all of these cases, the K_m for NADPH in the wild-type enzyme is approximately three orders of magnitude smaller than the K_m for NADH, in contrast with the 5-fold difference between the two in wild-type XR. An intermediate situation exists for aflatoxin reductase (AKR7A1), which exhibits a 180-fold lower K_m for NADPH compared with NADH [15]. The crystal structure that we describe in the present study demonstrates the molecular interactions that mediate this dual specificity in XR.

EXPERIMENTAL

Crystallization and data collection

XR was expressed and purified as described previously [16,17]. The buffer was exchanged to 10 mM Tris/HCl (pH 7.5) and the protein concentrated to 14 mg/ml. Crystals were grown at room temperature by suspending a drop of 7 mg/ml XR/2.5 mM NAD$^+$/16 % (w/v) poly(ethylene glycol) 5000-molecular-mass monomethyl ether/175 mM ammonium sulphate/50 mM sodium citrate (pH 5.6) over a well containing well solution [32 % (w/v) poly(ethylene glycol) 5000-molecular-mass monomethyl ether/350 mM ammonium sulphate/100 mM sodium citrate (pH 5.6)]. A single crystal was transferred to a cryo-protectant consisting of 75 % (v/v) well solution/25 %(v/v) ethylene glycol/2 mM NAD$^+$ before flash-cooling in a nitrogen stream (100 K). Data were collected at Stanford Synchrotron Radiation Laboratory beamline 9-1 on a MAR Research 345 detector and integrated and merged with DENZO and SCALEPACK [18]. Data collection statistics are presented in Table 1. Systematic extinctions indicated the spacegroup was $C2$ with unit cell dimensions $a = 180.20$ Å, $b = 128.34$ Å, $c = 79.95$ Å and $\beta = 90.75°$, similar to the unit cell determined for the NADP$^+$-bound form, but different from that seen in the crystals of the apoenzyme [5].

Structure determination and refinement

The unit cell was most similar to the unit cell of an XR His^{114} → Ala mutant crystal in a binary complex with NADP$^+$ (K. L. Kavanagh, M. Klimacek, B. Nidetzky and D. K. Wilson, unpublished results). This mutant structure was stripped of water molecules and used as a starting model. Before any refinement was performed, 8175 reflections were flagged for the calculation of a free R-factor. Difference density clearly indicated the absence of the 2′-phosphate on the adenosine ribose as well as several side-chain and main-chain conformational differences. Water molecules were automatically picked in CNS and manually checked for appropriate hydrogen-bonding and electron density. Alternating rounds of crystallographical refinement and manual refitting using the programs CNS and O resulted in the final model [19]. The statistics associated with the final round of refinement are summarized in Table 1.

Table 1 Summary of XR data collection, refinement and models

The high-resolution shell is 1.83–1.80 Å. r.m.s., root mean square.

Parameter	Values
Data collection	
Space group	$C2$
Unit cell	$a = 180.20$ Å
	$b = 128.34$ Å
	$c = 79.95$ Å
	$\beta = 90.75°$
Monomers per asymmetric unit	4
Resolution range (Å)	30–1.8
Number of observations/unique reflections	728 917/162 716
R_{merge} (overall/high resolution shell)	0.063/0.359
Completeness (overall/high resolution shell) (%)	98.9/98.2
Mosaicity (°)	0.29
$I/\sigma(I)$ (overall/high resolution shell)	13.04/3.02
Model	
Protein atoms	10 128
NAD$^+$ atoms	176
Water molecules	873
Refinement	
Reflections used ($I > 0$)	154 541
R_{cryst}	0.183
R_{free}	0.212
r.m.s. deviation from ideal bond length (Å)	0.018
r.m.s. deviation from ideal bond angle (°)	1.7

RESULTS

Overall structure

The enzyme folds into the $(\beta/\alpha)_8$ barrel, which has been described previously for XR [5] and other AKRs (Figure 1). There are four XR molecules (two dimers) within the crystallographical asymmetric unit. Each of the models consists of residues 4–322 out of the 322 residues predicted for the protein. Numbering starts with 1 for the initiator methionine, which is processed off in the mature protein. Also observed in the asymmetric unit are 873 ordered water molecules and an NAD$^+$ co-substrate clearly bound to each monomer. A Ramachandran plot generated by PROCHECK indicates that 90.9 % of the residues are in the core areas and 9.1 % are in allowed regions [20]. The average refined temperature factors are 22.2, 17.9, 20.3 and 13.8 Å^2 for molecules A–D respectively. The root mean square (r.m.s.) deviations between the C_α values of the models range from 0.14–0.30 Å, indicating that all of the molecules are virtually identical. Since the overall temperature factor for molecule D is the lowest, measurements and the majority of conclusions regarding specific atomic interactions were drawn from it.

Co-substrate binding and associated conformational change

The NAD$^+$ co-substrate binds across the carboxyl end of the inner β-barrel of the enzyme with the nicotinamide at the centre and the adenosine extended between repeats 7 and 8 in a manner similar to that seen for other AKRs. All of the non-hydrogen atoms in the NAD$^+$ are unambiguously observed in the final unbiased high-resolution electron density map (Figure 2, upper panel). Refined B-factors for individual co-substrate atoms in molecule D range from 7.7–14.4 Å^2, indicating that it is well-ordered. The nicotinamide portion of the NAD$^+$ co-substrate is bound in a manner virtually identical with that seen in the NADP$^+$-bound form. The adenine ring binds in a conserved hydrophobic pocket

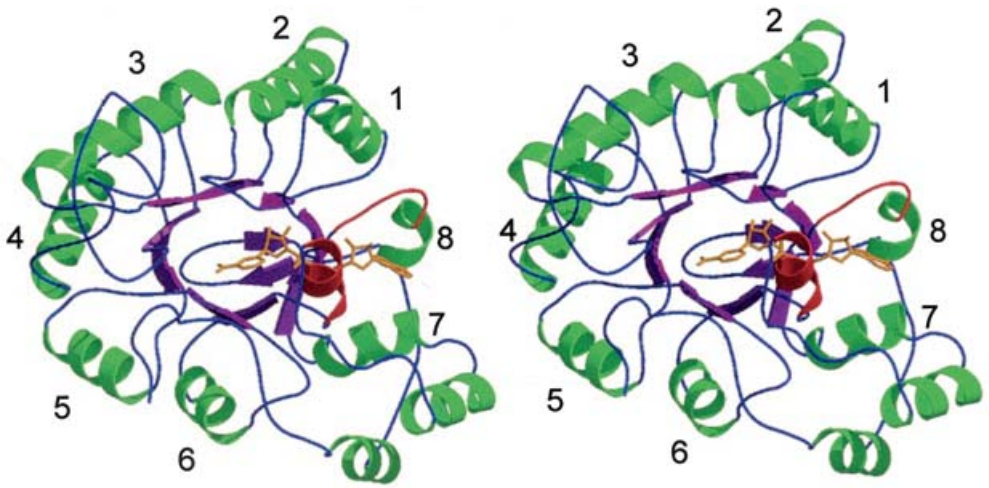

Figure 1 A stereo-view of the overall fold of XR

The individual β/α repeats are numbered next to each helix. The region of loops 7 and 8 undergoing the co-substrate-dependent conformational change are highlighted in red. Other regions of the protein are coloured green for helices, purple for strands and blue for loops. All Figures were generated using BOBSCRIPT [32] and rendered using Raster3D [33].

formed by Phe^{220}, Phe^{240} and Ala^{257} on one side. The other side of the adenosine stacks against the positively charged guanidinium group of Arg^{280}. Important differences in interactions that are responsible for dual substrate specificity are noted, however, when the mode of binding of the adenosine ribose is examined.

As would be expected, the differences between the NAD$^+$- and NADP$^+$-bound forms of the enzyme are localized. Molecule D of the NAD$^+$-bound form of XR was compared with molecule B of the NADP$^+$-bound XR (Protein Data Bank accession number 1K8C), which has the lowest average temperature factors of the four molecules in each asymmetric unit in that structure. The r.m.s. deviations of the C_α values between these two models was calculated to be 0.3 Å. Comparable values are obtained in most other pair-wise comparisons. Superimpositions of the models show the largest deviations between the two structures occur in the region surrounding the 2′-phosphate on the adenosine ribose (Figure 3). These are located primarily in two sequences. The first and largest of the conformational change is seen in residues 274–280, which form part of the loop in the eighth β/α repeat. The second involves a smaller, but significant, shift in residues 225–229, a short helical region that appears at the end of β7 (Figure 2, lower panel). The largest main-chain shift is seen in Ser^{275}, which moves 2.0 Å in response to the loss of the phosphate.

When the NAD$^+$-bound structure is compared with the structure of the apo form of the enzyme, a co-substrate-induced conformational change is observed, which orders the residues composing loop 7 (approx. residues 220–237), the region between β7 and α7 secondary structural motifs (Figure 1). This conformational change, which is probably largely due to the binding of the adenosine portion of the molecule, is also observed when NADP$^+$ binds to the enzyme [5]. Other significant conformational changes are observed in loop 8 (272–284) as well. Observed main-chain shifts of this loop are in the range of 1–3.5 Å.

In the co-substrate-bound form, the 4-*pro*-R position of the nicotinamide ring is presented for hydride transfer to the substrate carbonyl carbon, agreeing with the biochemically observed stereospecificity of XR [21]. Tyr^{52} functions as a general acid in the reduction reaction and is activated by Lys^{81} and Asp^{47} which complete a catalytic triad, similar to that seen in other AKRs. These residues are in a conformation identical with the NADP$^+$-bound structure, indicating that the catalytic mechanism is preserved.

The carbonyl-containing substrate-binding site is formed by residues flanking the invagination on top of the A face of the nicotinamide of the substrate. This surface is potentially formed by residues from either loops or β-strands from repeats 1, 2, 3 and 4 and several residues from the C-terminal loop of the enzyme. In addition, the co-substrate-induced conformational change moves several residues from loop 7 thereby completing the active site [5].

Differences in co-substrate binding and conformation

Although the main-chain conformational change is relatively modest, there is a great deal of unexpected side-chain rearrangement accompanying the removal of the co-substrate phosphate. On loop 8, the side chain of Lys^{274}, which interacted directly with the 2′-phosphate in NADP$^+$, rotates away slightly and is re-directed to hydrogen bond with solvent molecules. The Asn^{276} side chain, which made a long 3.41 Å hydrogen bond with a phosphate oxygen, rotates towards the ribose to form a 3.02 Å hydrogen bond with the 2′-oxygen in which its amide nitrogen functions as a donor. This side chain occupies the former site of the 2′-phosphate (Figure 3). In making this interaction in the NAD$^+$ complex, the hydrogen bond between the phosphate oxygen and the Asn^{276} main-chain NH is lost. The positively charged side chain of Arg^{280} shifts approx. 0.7 Å towards the 2′-oxygen. In the NADP$^+$-bound structure, it established a salt link with a phosphate oxygen and was also 3.44 Å from the 2′-hydroxy oxygen. In the NAD$^+$-bound structure, the shift allows it to form a hydrogen bond 3.13 Å from the 2′-hydroxy group. Its position is probably conserved due to the stacking interactions the guanidinium group makes with the purine ring of the adenosine, which has been seen in previous AKR structures from families 1 [22], 3 [22a] and 5 [22b]. Positions of Ser^{275} and other residues composing the loop are perturbed as a result of these changed interactions, but make no direct interactions themselves.

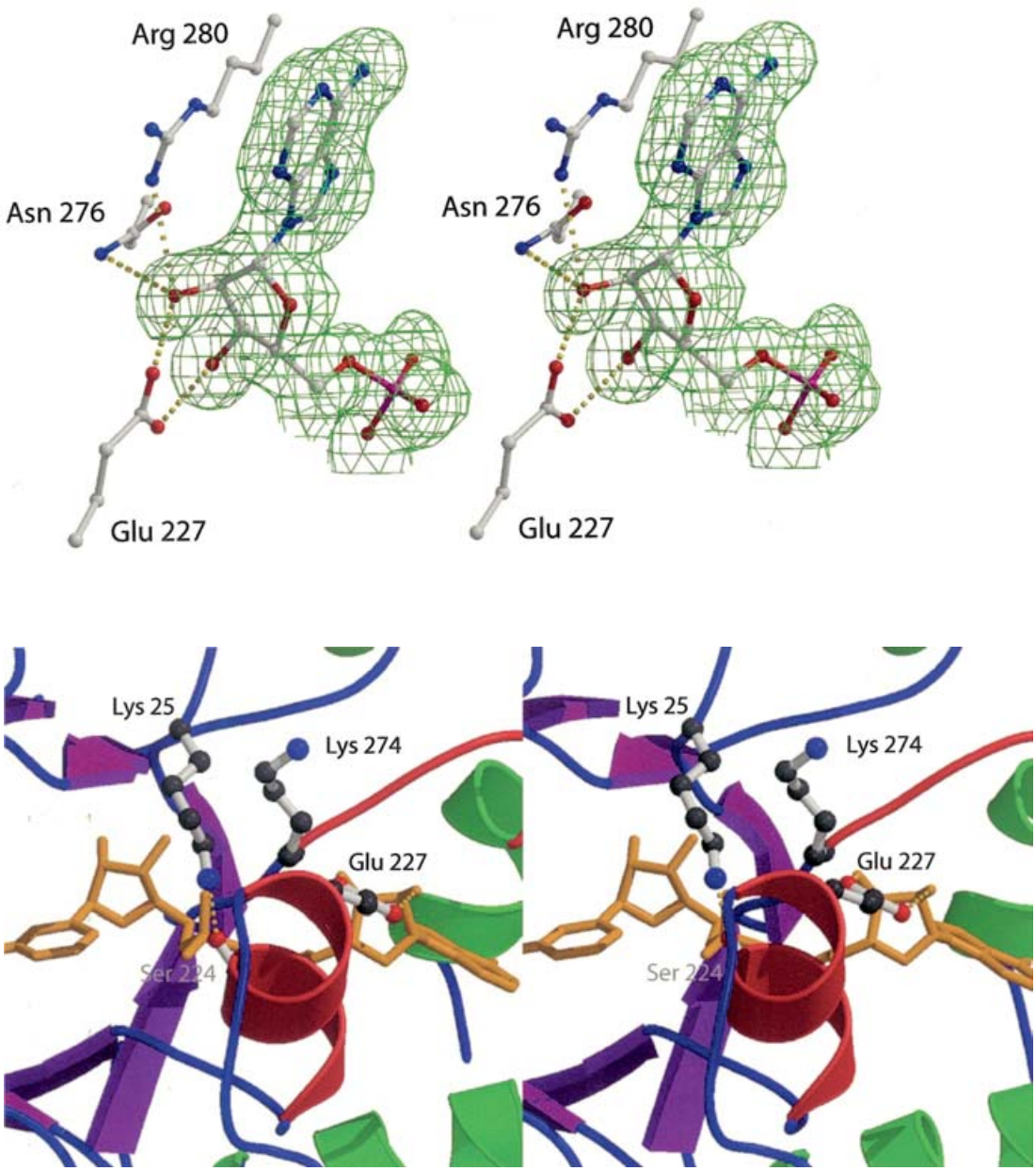

Figure 2 Co-substrate binding to XR

Upper panel: $|F_o\text{-}F_c|$ electron density contoured at 3σ corresponding to the adenosine region of the NAD^+-bound enzyme. Phases were derived from the refined model with the NAD^+ atoms removed. Lower panel: the location of Glu^{227} on a helix constrains the positioning of the side chain such that it is unable to establish the salt links with Lys^{25} and Lys^{274}, which are present in a number of other AKRs. As a result, Glu^{227} is available to hydrogen bond with the 2′- and 3′-hydroxy groups. The orientation is the same as in Figure 1.

The key interaction made from the other segment in the region between $\beta 7$ and $\alpha 7$ comes from Glu^{227}. In the $NADP^+$-bound structure, Glu^{227} and Lys^{274} make water-mediated interactions with each other and with the 3′-hydroxy group. These interactions are lost in the NAD-bound structure and the Nζ of Lys^{274} interacts with the bulk solvent instead. In the absence of a negatively charged phosphate when NAD^+ is bound, the Glu^{227} side chain is able to rotate into a favourable conformation to accept a 2.64 Å hydrogen bond with the 2′-hydroxy group and a 2.65 Å hydrogen bond with the 3′-hydroxy group (Figure 3).

As discussed above, two loops providing side chains involved in the ribose-binding site have undergone a conformational change, substantially changing its chemical and steric environment. The major effect this has on the co-substrate is that the sugar pucker for the adenosine ribose switches from the 2′-*endo* conformation (in which the 2′-carbon is on the 5′-carbon side of the *quasi*-plane formed by the other four ring atoms) for the $NADP^+$-bound complex to the 3′-*endo* conformation for the NAD^+-bound complex. It appears that this is a consequence of the loss of the phosphate interactions with the Ser^{275} side chain and the main-chain amide nitrogen from Asn^{276}, both of which served to promote the 2′-*endo* conformation. The change in sugar puckering also requires a change in the torsion angle between the adenosine C5 and O5, leading to a slightly different conformation in the

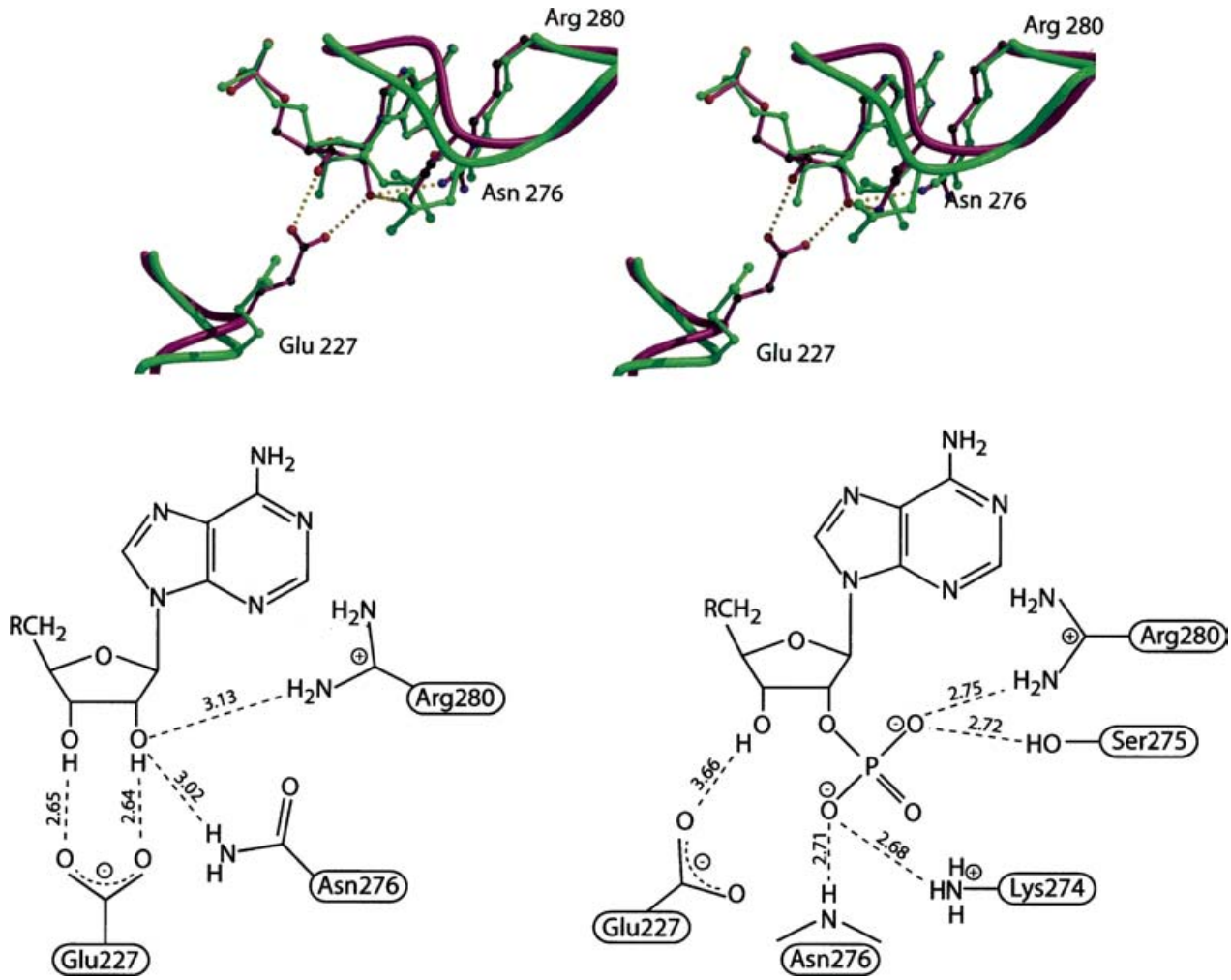

Figure 3 Comparison of XR–NADP+ and XR–NAD+ complexes

Upper panel: a stereo-view of the overlap of the NAD+- and NADP+-bound structures illustrating regions involved in conformational changes on loops 7 and 8. The complex with NAD+ is coloured purple for portions of the main chain trace and individual bonds. The NADP+ complex is coloured green for atoms, bonds and the main chain trace. The ribose pucker can be seen changing from 2′-*endo* in the complex with NADP+ to 3′-*endo* in the complex with NAD+. Lower left-hand panel: schematic diagram showing the interactions with the adenosine ribose 2′- and 3′-hydroxy groups in the complex with NAD+. Lower right-hand panel: schematic diagram of the interactions with the adenosine ribose 2′- and 3′-hydroxy groups and 2′-phosphate in the complex with NADP+ (PDB accession 1K8C). Distances are given in Å in the lower panels.

region between the sugar ring and the phosphate. Since this pucker affects the placement of the C5 atom, and the 5′-phosphorus is in an invariant position (Figure 3), this angle must undergo a large change from $-157°$ in the NADP+-bound structure to 175° in the NAD+-bound structure.

DISCUSSION

Why are most AKRs specific for NADPH, whereas XR can efficiently utilize either NADPH or NADH? To address this question, we compared the structure of the NADPH-specific AR (AKR1B1) bound to NADPH (Protein Data Bank accession number 1ADS) with XR bound to both co-substrates. The ability of XR to undergo key side-chain conformational rearrangements and to make alternate interactions with the 2′- and 3′-hydroxy groups in the absence of the 2′-phosphate appears to be the answer. In addition to this, extra secondary structural elements are present in XR which constrain the main-chain conformation and also aid in the dual specificity.

Residues Glu[227] and Asn[276] primarily mediate the interactions with the adenosine ribose 2′- and 3′-hydroxy groups. The more important of these two is the carboxylate of Glu[227], which forms a bidentate hydrogen bond with both of the hydroxy groups. Similar interactions have been noted in many other NADH-binding protein structures [23]. The structurally equivalent residues in AR, Asp[216] and Val[264], are unable to fulfil equivalent roles. In AR, Asp[216] is required for the high-affinity binding of the co-substrate but, surprisingly, does not make any critical contacts with the co-substrate itself. When NADP+ is bound, the side chain is engaged in two salt linkages with Lys[21] and Lys[262] thereby fastening a loop or ‘safety belt’ of residues over the co-substrate that are important in binding and have kinetically measurable consequences [22]. Similar belt-fastening interactions have been noted in structures of other AKRs and appear to play an important role in co-substrate binding in these as well. In XR, Glu[227] occupies space on a very short helical region, apparently unique to AKR family 2, which provides rigidity, thus preventing a similar interaction with the lysine residues that are conserved. The aspartate residue in AR

Table 2 Co-substrate usage and the presumed role of the carboxylate-containing residue equivalent to Glu^{227} in XR, poised to hydrogen bond with the 2′-and 3′-hydroxy groups of NADH in XR among representative AKRs

Conclusions were drawn based on structures, except in the cases of AKR2B1 and AKR2B3, which are based on sequence alignments. N.D., not detectable.

Enzyme	Organism	Activity	K_m^{NADPH}	K_m^{NADH}	Carboxylate	Ref.
AKR1B1	*Homo sapiens*	Aldose reductase	2.9 μM	1.2 mM	Binds lysines to form belt	[12]
AKR1C9	*Rattus norvegicus*	3α-Hydroxysteroid dehydrogenase	1.9 μM	39.8 μM	Interacts with Glu^{27} main-chain amide nitrogen; approx. 9 Å from 3′-hydroxy group	[14]
AKR2B1	*Pichia stipitis*	XR	9 μM	21 μM	Presumably binds 2′- and 3′-hydroxy groups	[24]
AKR2B3	*Pachysolen tannophilus*	XR	21 μM	40 μM	Presumably binds 2′- and 3′-hydroxy groups	[25]
AKR2B5	*Candida tenuis*	XR	4.8 μM	25.4 μM	Interacts with 2′- and 3′-hydroxy groups	[3]
AKR3A	*Saccharomyces cerevisiae*	Aldose reductase	28.5 μM	N.D.	Asp^{226} 9 Å from 2′- and 3′-hydroxy groups	[34]
AKR5C	*Corynebacterium*	2,5 Diketo-gluconate reductase	10 μM	2.4 mM	No structurally equivalent carboxylate	[35,36]
AKR7A1	*R. norvegicus*	Aflatoxin reductase	2.6 μM	480 μM	Glu^{216} 10 Å from 2′- and 3′-hydroxy groups	[15]

is on a more flexible loop, which allows it the conformational freedom necessary to form salt links with the lysine residues. A similar situation is seen in the majority of other AKRs that have been structurally characterized in the holo form. In these cases, the carboxylate is therefore unavailable to make the important interactions with the ribose 2′- and 3′-hydroxy groups.

As a result of a four amino acid insert in XR that forms a short helix, Glu^{227} is somewhat displaced from the position Asp^{216} occupies in AR and is therefore unable to make the salt bridge bridging the co-substrate and fastening it into its binding site (Figure 2, lower panel). This insertion appears to be unique to AKR family 2 (Table 2). The distances from the nearest carboxylate oxygen in Glu^{227} to the Lys^{25} and Lys^{274} Nζ atoms are 4.03 Å and 4.25 Å respectively. Rather than engaging in this salt link, Lys^{25} hydrogen bonds to Ser^{224} to preserve what may be a weaker 'safety belt' interaction across the co-substrate. This may be responsible for the lower affinity of NADPH exhibited by XR when compared with AR. A glutamate residue is found at the position analogous to 227 in XR in nine of the 14 family 2 members. Outside of the family, there is very little conservation at this position, most notably in AKR1C9, a protein with known dual co-substrate specificity.

The side chain of Asn^{276} in XR, which makes a single hydrogen bond with the ribose, is replaced by Val^{264} in AR. This is obviously unable to make the necessary hydrogen-bonding interactions with the 2′-hydroxy group to mediate NADH binding. Thr^{265}, which hydrogen bonds to the 2′-phosphate in AR, might be considered as an alternate possibility to potentially hydrogen bond with the 2′-hydroxy group in NADH. Since the threonine residue side chain is shorter than an asparagine residue, the protein would be required to flex into an unfavourable conformation to place the threonine residue side chain into a position where it could hydrogen bond. Asn^{276} appears to be conserved in six of the 14 members of family 2; however, it is very poorly conserved outside of the family.

Enumerating the number of hydrogen bonds made in each complex or potential complex summarizes the effects of the 2′-phosphate on co-substrate binding. XR–NADP$^+$ makes four hydrogen bonds (two charged) with the adenosine ribose and phosphate atoms. In XR, the loss of the phosphate causes a conformational change in the enzyme, which is still able to accommodate the ribose with a total of four hydrogen bonds, three to the 2′-hydroxy group and one to the 3′-hydroxy group.

In contrast, AR makes a total of six hydrogen bonds (two charged) with the ribose and phosphate. Its binding site is not able to accommodate the loss of the phosphate and is probably only able to make a single hydrogen bond from Arg^{268} to the 2′-hydroxy group in the hypothetical complex. The nicotinamide engages in seven hydrogen bonds as well as stacking interactions with Tyr^{217}, which orient and tightly bind the nicotinamide ring and ensure stereospecific hydride transfer. Despite these, the interactions with the adenosine ribose or adenosine ribose phosphate are critical for effective use of the co-substrate.

Using sequence information in the absence of structure to determine co-substrate specificity is probably not possible in a straightforward manner for the majority of AKRs outside of family 2. Within family 2, the XRs from *Pichia stipitis* (AKR2B1) and *Pachysolen tannophilus* (AKR2B3) also exhibit clear dual co-substrate specificity [24,25]. There is conflicting information, however, regarding XR from *Candida tropicalis* (AKR2B4). One report suggests that it is specific for NADPH [26], whereas others show dual specificity [27,28]. Since a key determinant for NADH specificity appears to be Glu^{227} in *C. tenuis* XR, we examined this position in the other XRs. Residues in all four enzymes are well conserved in this region, suggesting that the tertiary structure is also conserved.

Outside of family 2, most other structurally characterized AKRs bind NADH weakly (>1 mM affinity), with the exception of aflatoxin reductase (AKR7A1), which utilizes NADH slightly more efficiently with a K_m of 480 μM [15], and rat 3α-hydroxysteroid dehydrogenase (AKR1C9), with a K_m of 39.8 μM [14]. Aflatoxin reductase is similar to XR in much of the main-chain trace and in its ability to form dimers. The general mode of co-substrate binding is also fairly well conserved, but the atomic interactions mediating adenosine 2′-phosphate binding are divergent [29]. There are several possibilities for which residues make contact with the 2′- and 3′-hydroxy groups in a putative NAD(H)-bound AKR7A1 model, but none appear to be optimal. One possibility includes Glu^{216}, the residue structurally homologous with Glu^{227} in XR. To make effective hydrogen bonds with the sugar oxygen, its carboxylate would have to move more than 10 Å, displacing numerous residues in the region. For this reason, it is too speculative to attempt to predict conformational rearrangements that might accompany NADH binding in AKR7A1.

AKR1C9 has Asp^{224} which might be considered homologous in function with Glu^{227} in XR based on sequence alone, but several factors may make this difficult. Based upon the structure of the AKR1C9 ternary complex with NADP$^+$ and testosterone [30], the shorter side chain of the aspartate residue and slightly different placement position of the nearest carboxylate oxygen is 8.99 Å from the adenosine O3′ compared with 3.66 Å for the analogous distance of the glutamate residue side chain in the XR complex

with $NADP^+$. The Asp^{224} side chain is also engaged in a hydrogen bond with the main-chain amide nitrogen of Glu^{27}. Glu^{227} in XR makes no such interactions which may facilitate it making interactions with the adenosine ribose. Furthermore, the loop in AKR1C9 containing Asp^{224} is in a different conformation and makes different interactions, which may preclude the structural rearrangement seen upon NAD^+ binding.

An effort to engineer an NADH-specific 2,5-diketo-D-gluconic acid reductase (AKR5C) from *Corynebacterium* for commercial purposes has yielded a quadruple mutant enzyme that improves NADH utilization by two orders of magnitude [11]. The mutations, $Phe^{22} \rightarrow Tyr$, $Lys^{232} \rightarrow Gly$, $Arg^{238} \rightarrow His$ and $Ala^{272} \rightarrow Gly$ are widely distributed about the dinucleotide-binding site and none would appear to facilitate the introduction of a carboxylate residue to interact with the adenosine 2′- and 3′-hydroxy groups. We therefore conclude that the NADH specificity determinants in this enzyme are different from those that we observe in XR.

A porcine aldehyde reductase mutant lacking eight residues in the C-terminal loop has been characterized, which confers an impressive conversion of enzyme specificity from NADPH (wild-type $K_m = 3.7\ \mu M$; mutant $K_m = 670\ \mu M$) into NADH (wild-type $K_m = 5100\ \mu M$; mutant $K_m = 35\ \mu M$) [31]. In the absence of a NAD(H)-bound crystal structure for this enzyme, it is very difficult to reconcile this biochemical data with the changes in the primary structure, because none of the residues make direct contact with the co-substrate in the $NADP^+$-bound holoenzyme structure. Despite the magnitude of changes in substrate specificity, the structural effects of the deletion may therefore be secondary.

The structure of XR bound to NAD^+ illustrates the unpredictable changes in the protein upon binding of a substrate, despite the fact that a highly homologous structure of the protein bound to $NADP^+$ already existed. The unexpected role of Glu^{227} in binding the 2′- and 3′-hydroxy groups and the structural constraints placed upon it preventing the 'safety belt' interaction seen in other AKRs are demonstrated. Analogous residues can also be seen in other dual-specificity family 2 members. Despite the fact that other AKRs outside of family 2 are able to utilize NADH, they lack the carboxylate-containing residue critical for interaction with the 2′- and 3′-hydroxy groups and, therefore, catalyse the reaction with a lower efficiency using NADH or use alternative residues to mediate efficient utilization.

This work was supported by a grant from the National Institutes of Health to D.K.W., and the Keck Foundation. K.L.K. is supported by a grant from the University of California Systemwide Biotechnology Research Program, proposal number 2001-07. Further support to B.N. was provided by the Austrian Science Foundation (grant P-15208-MOB). The data collection facilities at Stanford Synchrotron Radiation Laboratory are funded by the U.S. Department of Energy and by the National Institutes of Health.

REFERENCES

1 Lee, H. (1998) The structure and function of yeast xylose (aldose) reductases. Yeast **14**, 977–984

2 Jez, J. M. and Penning, T. M. (2001) The aldo-keto reductase (AKR) superfamily: an update. Chem.–Biol. Interact. **130–132**, 499–525

3 Neuhauser, W., Haltrich, D., Kulbe, K. D. and Nidetzky, B. (1997) NAD(P)H-dependent aldose reductase from the xylose-assimilating yeast *Candida tenuis*. Biochem. J. **326**, 683–692

4 Kador, P. F., Robinson, W. G. and Kinoshita, J. H. (1984) The pharmacology of aldose reductase inhibitors. Annu. Rev. Pharmacol. Toxicol. **25**, 691–714

5 Kavanagh, K. L., Klimacek, M., Nidetzky, B. and Wilson, D. K. (2002) The structure of apo and holo forms of xylose reductase, a dimeric aldo-keto reductase from *Candida tenuis*. Biochemistry **41**, 8785–8795

6 Branden, C. I. (1991) The TIM barrel: the most frequently occurring folding motif in proteins. Curr. Opin. Struct. Biol. **1**, 978–983

7 Hahn-Hagerdal, B., Wahlbom, C. F., Gardonyi, M., van Zyl, W. H., Otero, R. R. C. and Jonsson, L. J. (2001) Metabolic engineering of *Saccharomyces cerevisiae* for xylose utilization. Adv. Biochem. Eng./Biotechnol. **73**, 53–84

8 Lunzer, R., Mamnun, Y., Haltrich, D., Kulbe, K. D. and Nidetzky, B. (1998) Structural and functional properties of a yeast xylitol dehydrogenase, a Zn^{2+}-containing metalloenzyme similar to medium-chain sorbitol dehydrogenases. Biochem. J. **336**, 91–99

9 Ostergaard, S., Olsson, L. and Nielsen, J. (2000) Metabolic engineering of *Saccharomyces cerevisiae*. Microbiol. Mol. Biol. Rev. **64**, 34–50

9a Senac, T. and Hahn-Hagerdal, B. (1991) Effects of increased transaldolase activity on D-xylulose and D-glucose metabolism in *Saccharomyces cerevisiae* cell extracts. Appl. Environ. Microbiol. **57**, 1701–1706

10 Neuhauser, W., Haltrich, H., Kulbe, K. D. and Nidetzky, B. (1998) Noncovalent enzyme-substrate interactions in the catalytic mechanism of yeast aldose reductase. Biochemistry **37**, 1116–1123

11 Banta, S., Swanson, B. A., Wu, S., Jarnagin, A. and Anderson, S. (2002) Optimizing an artificial metabolic pathway: engineering the cofactor specificity of *Corynebacterium* 2,5-diketo-D-gluconic acid reductase for use in vitamin C biosynthesis. Biochemistry **41**, 6226–6236

12 Kubiseski, T. J. and Flynn, T. G. (1995) Studies on human aldose reductase: probing the role of arginine 268 by site-directed mutagenesis. J. Biol. Chem. **270**, 16911–16917

13 Matsuura, K., Tamada, Y., Sato, K., Iwasa, H., Miwa, G., Deyashiki, Y. and Hara, A. (1997) Involvement of two basic residues (Lys-270 and Arg-276) of human liver 3α-hydroxysteroid dehydrogenase in NADP(H) binding and activation by sulphobromophthalein: site-directed mutagenesis and kinetic analysis. Biochem. J. **322**, 89–93

14 Ratnam, K., Ma, H. and Penning, T. M. (1999) The arginine 276 anchor for NADP(H) dictates fluorescence kinetic transients in 3α-hydroxysteroid dehydrogenase, a representative aldo-keto reductase. Biochemistry **38**, 7856–7864

15 Ellis, E. M. and Hayes, J. D. (1995) Substrate specificity of an aflatoxin-metabolizing aldehyde reductase. Biochem. J. **312**, 535–541

16 Haecker, B., Habenicht, A., Kiess, M. and Mattes, R. (1999) Xylose utilisation: cloning and characterisation of the xylose reductase from *Candida tenuis*. Biol. Chem. **380**, 1395–1403

17 Mayr, P., Brueggler, K., Kulbe, K. D. and Nidetzky, B. (2000) D-Xylose metabolism by *Candida intermedia*: isolation and characterisation of two forms of aldose reductase with different coenzyme specificities. J. Chromatogr. B Biomed. Sci. Appl. **737**, 195–202

18 Otwinowski, Z. and Minor, W. (1997) Processing of X-ray diffraction data collected in oscillation model. Methods Enzymol. **276**, 307–326

19 Brünger, A. T., Adams, P. D., Clore, G. M., DeLano, W. L., Gros, P., Grosse-Kunstleve, R. W., Jiang, J. S., Kuszewski, J., Nilges, M., Pannu, N. S. et al. (1998) Crystallography & NMR system: a new software suite for macromolecular structure determination. Acta Crystallogr. D Biol. Crystallogr. **54**, 905–921

20 Laskowski, R. A., MacArthur, M. W., Moss, D. S. and Thornton, J. M. (1993) PROCHECK: a program to check the stereochemical quality of protein structures. J. Appl. Crystallogr. **26**, 283–291

21 Nidetzky, B., Mayr, P., Neuhauser, W. and Puchberger, M. (2001) Structural and functional properties of aldose xylose reductase from the D-xylose-metabolizing yeast *Candida tenuis*. Chem.–Biol. Interact. **130–132**, 583–595

22 Wilson, D. K., Bohren, K. M., Gabbay, K. H. and Quiocho, F. A. (1992) An unlikely sugar substrate site in the 1.65 Å structure of the human aldose reductase holoenzyme implicated in diabetic complications. Science (Washington, D.C.) **257**, 81–84

22a Hur, E. and Wilson, D. K. (2001) The crystal structure of the GCY1 protein from *Saccharomyces cerevisiae* suggests a divergent aldo-keto reductase catalytic mechanism. Chem. Biol. Int. **130**, 527–536

22b Sanli, G. and Blaber, M. (2001) Structural assembly of the active site in an aldo-keto reductase by NADPH cofactor. J. Mol. Biol. **309**, 1209–1218

23 Carugo, O. and Argos, P. (1997) NADP-dependent enzymes. I: conserved stereochemistry of cofactor binding. Proteins Struct. Funct. Genet. **28**, 10–28

24 Verduyn, C., van-Kleef, R., Frank, J., Schreuder, H., van-Dijken, J. P. and Scheffers, W. A. (1985) Properties of the NAD(P)H-dependent xylose reductase from the xylose-fermenting yeast *Pichia stipitis*. Biochem. J. **226**, 669–677

25 Verduyn, C., van-Dijken, J. P. and Scheffers, W. A. (1985) Multiple forms of xylose reductase in *Pachysolen tannophilus* CBS4044. FEMS Microbiol. Lett. **30**, 313–317

26 Yokoyama, S.-I., Suzuki, T., Kawai, K., Horitsu, H. and Takamizawa, K. (1995) Purification, characterization and structure analysis of NADPH-dependent D-xylose reductases from *Candida tropicalis*. J. Ferment. Bioeng. **79**, 217–223

27 Horitsu, H., Yahashi, Y., Takamizawa, K., Kawai, K., Suzuki, T. and Watanabe, N. (1992) Production of xylitol from D-xylose by *Candida tropicalis*: optimization of production rate. Biotechnol. Bioeng. **40**, 1085–1091

28 Granstrom, T. and Leisola, M. (2002) Controlled transient changes reveal differences in metabolite production in two *Candida* yeasts. Appl. Microbiol. Biotechnol. **58**, 511–516
29 Kozma, E., Brown, E., Ellis, E. M. and Lapthorn, A. J. (2002) The crystal structure of rat liver AKR7A1: a dimeric member of the aldo-keto reductase superfamily. J. Biol. Chem. **277**, 16285–16293
30 Bennett, M. J., Schlegel, B. P., Jez, J. M., Penning, T. M. and Lewis, M. (1996) Structure of 3α-hydroxysteroid/dihydrodiol dehydrogenase complexed with $NADP^+$. Biochemistry **35**, 10702–10711
31 Rees-Milton, K. J., Jia, Z., Green, N. C., Bhatia, M., El-Kabbani, O. and Flynn, T. G. (1998) Aldehyde reductase: the role of C-terminal residues in defining substrate and cofactor specificities. Arch. Biochem. Biophys. **355**, 137–144
32 Esnouf, R. M. (1997) An extensively modified version of Molscript that includes greatly enhanced colouring capabilities. J. Mol. Graphics **15**, 113–138
33 Merritt, E. A. and Bacon, D. J. (1997) Raster3D: photorealistic molecular graphics. Methods Enzymol. **277**, 505–524
34 Hur, E. and Wilson, D. K. (2000) Crystallization and aldo-keto reductase activity of Gcy1p from *Saccharomyces cerevisiae*. Acta Crystallogr. D Biol. Crystallogr. **56**, 763–765
35 Miller, J. V., Estell, D. A. and Lazarus, R. A. (1987) Purification and characterization of 2,5-diketo-D-gluconate reductase from *Corynebacterium* sp. J. Biol. Chem. **262**, 9016–9020
36 Banta, S., Swanson, B. A., Wu, S., Jarnagin, A. and Anderson, S. (2002) Alteration of the specificity of the cofactor-binding pocket of *Corynebacterium* 2,5-diketo-D-gluconic acid reductase A. Protein Eng. **15**, 131–140

Received 19 February 2003/1 May 2003; accepted 6 May 2003
Published as BJ Immediate Publication 6 May 2003, DOI 10.1042/BJ20030286